AJNR

Diffusion-Weighted MR Imaging in a Rat Model of Syringomyelia after Excitotoxic Spinal Cord Injury

Eric D. Schwartz, Robert P. Yezierski, Pradip M. Pattany, Robert M. Quencer and Raymond G. Weaver

AJNR Am J Neuroradiol 1999, 20 (8) 1422-1428
http://www.ajnr.org/content/20/8/1422

AJNR Am J Neuroradiol 20:1422–1428, September 1999

Diffusion-Weighted MR Imaging in a Rat Model of Syringomyelia after Excitotoxic Spinal Cord Injury

Eric D. Schwartz, Robert P. Yezierski, Pradip M. Pattany, Robert M. Quencer, and Raymond G. Weaver

BACKGROUND AND PURPOSE: **Recent experimental data have shown that an increase of excitatory amino acids and the initiation of inflammatory responses within the injured spinal cord may play a role in post-traumatic syringomyelia. The purpose of this study was to determine whether diffusion-weighted MR imaging with apparent diffusion coefficient (ADC) maps could provide earlier evidence of spinal cord cavitation in a rat model of syringomyelia than available with conventional MR imaging.**

METHODS: **The spinal cord gray matter of four rats was injected with the α-amino-3 hydroxy-5 methyl-4 isoxazole propionic acid/metabotropic receptor agonist quisqualic acid. Animals were sacrificed at 1, 4, or 8 weeks after injection, and the spinal cords were fixed in formalin for 1 week and imaged with T1-, T2-, and diffusion-weighted sequences. One control specimen was also imaged. ADC maps were constructed from the diffusion-weighted data. Histopathologic analyses of sections stained with cresyl violet were compared with the MR images.**

RESULTS: **By 1 week after injection, ADC maps at the level of injection showed areas within the gray matter of increased intensity and increased ADC values as compared with the control specimen. These bright areas corresponded to cysts or cavities within the cord parenchyma on the histopathologic sections. The ADC values within affected gray matter areas progressively increased at 4 and 8 weeks, also corresponding to cyst formation. Conventional T1- and T2-weighted images showed corresponding lesions with cystic characteristics at 4 and 8 weeks, but not at 1 week.**

CONCLUSION: **In an animal model of syringomyelia, diffusion-weighted imaging with ADC maps detected cystic lesions within spinal cord gray matter before they were seen on conventional T1- and T2-weighted images.**

Post-traumatic syringomyelia affects up to 3% of patients with spinal cord injury and up to 8% of patients suffering from complete quadriplegia (1–4). Development of a symptomatic syrinx after injury takes from 2 months to 30 years (5, 6), with the most common initial complaint being pain (2, 5). Other symptoms and complications include sensory loss, motor weakness, increased or decreased spasticity, autonomic dysreflexia, hyperhidrosis (above the level of injury), sphincter loss or sexual dysfunction, Horner's syndrome, respiratory insufficiency, and death (1, 2). Currently, the most sensitive noninvasive imaging test for diagnosing posttraumatic syringomyelia and defining the morphology of a spinal cord cyst is conventional MR imaging (2, 5–9).

The pathogenesis of post-traumatic syringomyelia is not completely understood (1–4, 6, 7, 9–11). It has been shown in previous studies using experimental models of traumatic and ischemic spinal cord injury that, following injury, there is a significant increase in extracellular levels of excitatory amino acids, especially glutamate (12–16). The role of different glutamate receptor subtypes, including *N*-methyl-D-aspartate and α-amino-3 hydroxy-5 methyl-4 isoxazole propionic acid (AMPA) receptors, in the tissue-damaging effects of injury have been confirmed by the neuroprotective effects of specific receptor antagonists (17–20). In an effort to simulate the injury-induced changes in glutamate concentration and to evaluate the pathophysiologic consequences of this change, the technique of in-

Received October 26, 1998; accepted after revision March 29, 1999.

Supported in part by The Miami Project, Department of Defense, DAAH04-94-G-0425.

Presented at the annual meeting of the American Society of Neuroradiology, Philadelphia, May 1998.

From the Department of Radiology (E.D.S., P.M.P., R.M.Q.) and the Department of Neurosurgery and the Miami Project to Cure Paralysis (R.P.Y.), University of Miami School of Medicine; and Picker International Inc, MR Division, Highland Heights, OH (R.G.W.).

Address reprint requests to Eric D. Schwartz, MD, Department of Neuroradiology, University of Pennsylvania Medical Center, 3400 Spruce Street, Philadelphia, PA 19104.

traspinal microinjection was used to deliver agonists of specific glutamate receptor subtypes into the spinal gray matter (19, 21). In the present study, quisqualic acid (QUIS), an agonist of the AMPA/metabotropic receptor subtype, was used. QUIS was shown in a previous study to produce a dose- and time-dependent loss of neurons that led to the formation of cavities within the cord parenchyma (21). Similar injections with normal saline showed no cell loss or cyst formation. In addition to the excitotoxic effects of QUIS, other pathologic characteristics of this model include demyelination, astrocytic responses as measured by increased staining for glial fibrillary acidic factor, and a prominent inflammatory response (21–23). Thus, the excitotoxic (ie, QUIS) model of spinal cord injury shares many of the same characteristics as described in other models of traumatic and ischemic injury and, more important, as found after spinal cord injury in humans (24, 25).

Previous studies of spinal cord injury in rats both in vivo and in situ have shown that high-resolution MR imaging may be useful in helping to predict qualitatively and quantitatively the extent of an acute injury (26–29). Some of these investigations have shown qualitative changes in MR signal that correlated with histologic findings (26); others have quantified the extent of injury with MR imaging by measuring lesion length and volume (27–29). In another study, apparent diffusion coefficient (ADC) values were assessed in situ, and changes were seen in portions of the injured spinal cord that were not visible on conventional images (30). The animal models used in these studies included weight drop and clip compression.

While it was noted that cystic lesions might develop in these models, none of these studies specifically focused on predicting or imaging cystic lesions. In the present study, we used a model of post-traumatic syringomyelia to assess conventional T1- and T2-weighted imaging against diffusion-weighted imaging with ADC maps to determine whether the latter would provide evidence of cystic lesions before conventional T1- and T2-weighted imaging did.

Methods

Rat Model of Syringomyelia

The technique used for QUIS injections was similar to that described in previous studies using the method of intraspinal microinjection to produce spinal injury (21). Briefly, male Sprague-Dawley rats (250 to 300 g) were anesthetized with a mixture of ketamine, acepromazine, and xylazine (0.65 mL/kg, administered subcutaneously). After the vertebral column was exposed at T12–L2 and cleared of muscle and connective tissue, small portions of the vertebral lamina and spinous process were removed, and the dura was incised longitudinally and reflected bilaterally. At the site of the injection, the pia mater was carefully elevated using a No. 5 Dumont forceps and a small hole was made to allow penetration of the injection pipette. Glass micropipettes (tip diameter, 5 to 10 μm) attached to a Hamilton microliter syringe (volume, 5 μL) were used for the parenchymal injections. The syringe was mounted on a microinjector attached to a micromanipulator. Injections are made between the dorsal vein and dorsal root entry zone at depths ranging from 300 to 900 μm below the surface of the cord. These coordinates positioned the injection sites in the gray matter between laminae I and V. Stock solutions of 125 mM QUIS (RBI, Natick, MA) were made using normal saline. At each injection site, 0.1 μL of 125 mM QUIS was injected (over a 60-second interval). The total volume of QUIS ranged from 0.6 to 1.2 μL (three tracks per animal separated by 0.3 mm, bilateral injections). Based on the volumes injected, the total quantity of QUIS delivered at each injection site ranged from 0.1 to 0.6 μg. Following the injections, the muscles were closed in layers, the skin was closed with wound clips, and the animals were returned to their home cages.

A total of four rats were injected with QUIS for this study; two animals were sacrificed at 1 week, one was sacrificed at 4 weeks, and a fourth was sacrificed at 8 weeks. Initially, one animal was to be sacrificed at 2 weeks, but self-injurious grooming behavior, which developed after the spinal cord injection, necessitated sacrifice at 1 week. A fifth rat was sacrificed without having been injected with QUIS, and served as a control animal. Before sacrifice, animals were given an overdose of sodium pentobarbital. Sacrifice was performed with transcardial perfusion using buffered normal saline followed by 10% buffered formalin. The spinal cord was dissected and attached to a 2-mm dowel to ensure proper alignment. The spinal cords were then placed in a 10% formalin solution for 1 week before imaging.

MR Imaging

Spinal cords were imaged 1 week after fixation and storage. The spinal cords were removed from the formalin solution and placed over a 4-cm single-loop receiver coil in a 1.5-T magnet. The coil was centered over injection sites identified by examining the dorsal surface of the cord for dural and pial openings.

Axial T1-weighted (800/22/6 [TR/TE/excitations]) and T2-weighted (2000/80/4) images were obtained, and axial diffusion-weighted images (3000/130/1) were acquired with diffusion encoding applied along the slice-select (z) and read (x) axes. Five different b values of 0, 200, 400, 600, and 750 s/mm^2 were used along each of the two axes to obtain calculated ADC images. In all sequences, 12 axial images were obtained, with a section thickness of 3 mm, a field of view of 31 mm, and an image matrix of 200 $\times$ 200.

Histopathologic Analysis

After imaging, the specimens were sectioned and stained with cresyl violet. Cresyl violet (Nissl stain) strongly stains ribosomal RNA in the rough endoplasmic reticulum (Nissl substance) of the neuronal cytoplasm.

The formation of cystic lesions within the spinal cord parenchyma after injury may be divided into stages (31). In the first stage, 1 to 2 weeks after injury, a debris-filled necrotic zone forms, which may be referred to as a cavity. Following this stage, macrophages clear the debris and the cystic lesion is delineated by a wall of astrocytic processes, fibroblasts, and collagen; this fluid-filled lesion may now be described as a cyst. As the lesion progresses from cavity to cyst, it may enlarge until it reaches a stable size.

Image Analysis

Images were interpreted by consensus among the authors. The T1- and T2-weighted images were first evaluated for cyst formation. A cyst was defined as a lesion with CSF-equivalent intensity on T1- and T2-weighted sequences.

ADC maps depict Brownian motion, which is the process of random molecular diffusion in fluid. In organized biological

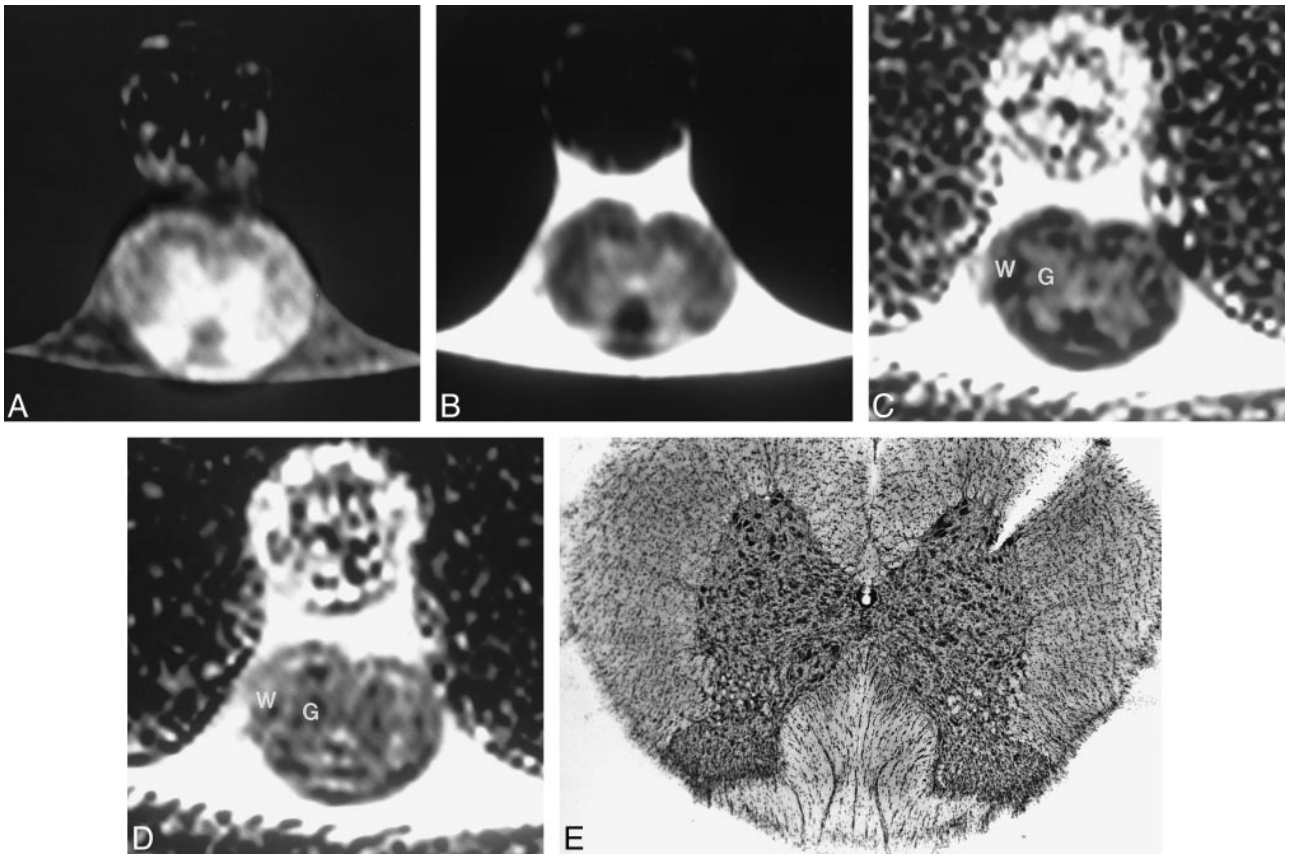

FIG 1. *A–E,* Cross-sectional T1-weighted (800/22/6) (*A*) and T2-weighted (2000/80/4) (*B*) images of the spinal cord control specimen show expected hypointensity of white matter on both imaging sequences. Cross-sectional ADC images of this same animal in the read (*C*) and slice-select (*D*) axes show gray (*G*)/white (*W*) differentiation. A 2-mm dowel is seen ventrally. As expected, the gray matter is relatively isointense on both images but the white matter shows longitudinal anisotropy; ie, hypointense on the read axis (*C*) and hyperintense on the slice-select axis (*D*). Corresponding histopathologic section (*E*) is provided for images shown in *A–D*; the notch in the upper left of the specimen is used to mark the left side of the spinal cord before sectioning.

structures, such as white matter tracts, diffusion properties are said to be anisotropic; that is, diffusion is more restricted in one direction than another. Isotropic refers to structures with diffusion properties equal in all directions. The ADC maps show increased signal when there is relatively unrestricted movement of water molecules in the plane of diffusion encoding and show decreased signal with relatively restricted motion of water molecules. Increased signal should be seen in a fluid-filled spinal cord cyst, as the movement of water molecules will be freer in fluid than in cellular structures. A necrotic spinal cord cavity should also display abnormally increased signal, as the free movement of water molecules should increase with cell destruction and necrosis. The increased signal should be seen in both planes of acquisition, as fluid movement should be isotropic in a cyst or cavity. The diffusion coefficient values, which are measured from the ADC maps, show increasing values with less restricted motion of water molecules.

The ADC maps were evaluated and compared with the routine MR and histopathologic images. To obtain ADC values, regions of interest were drawn around these areas of increased intensity in the ADC maps. ADC values were measured in both the slice-select and read axes.

Statistical Analysis

Statistical analyses were conducted to determine whether changes in ADC values among rats sacrificed at different times following injection were statistically significant. Linear regressions were performed with SPSS for Windows 7.5.1 (SPSS, Inc, Chicago, IL). *P* values of less than .05 were considered significant.

Results

Conventional T1- and T2-weighted images of the normal control specimen showed expected signal intensity for gray and white matter (Fig 1A and B). In both imaging sequences, gray/white matter differentiation was evident, and the gray matter was hyperintense relative to white matter. This finding is consistent with previous MR studies of the rat and human spinal cord and was thought to be due to the relatively small T1 and T2 differences between gray and white matter of the spinal cord, causing images to be dominated by the increased spin density of the gray matter (32). ADC maps of the control specimen showed gray/white differentiation in both the read and slice-select axes (Fig 1C and D), which corresponded to the histopathologic specimen (Fig 1E). In both axes, the spinal gray matter maintained an intermediate intensity. In the slice-select (z) axis, there was increased intensity of the white matter as compared with the gray matter, and in the read (x) axis, the white matter

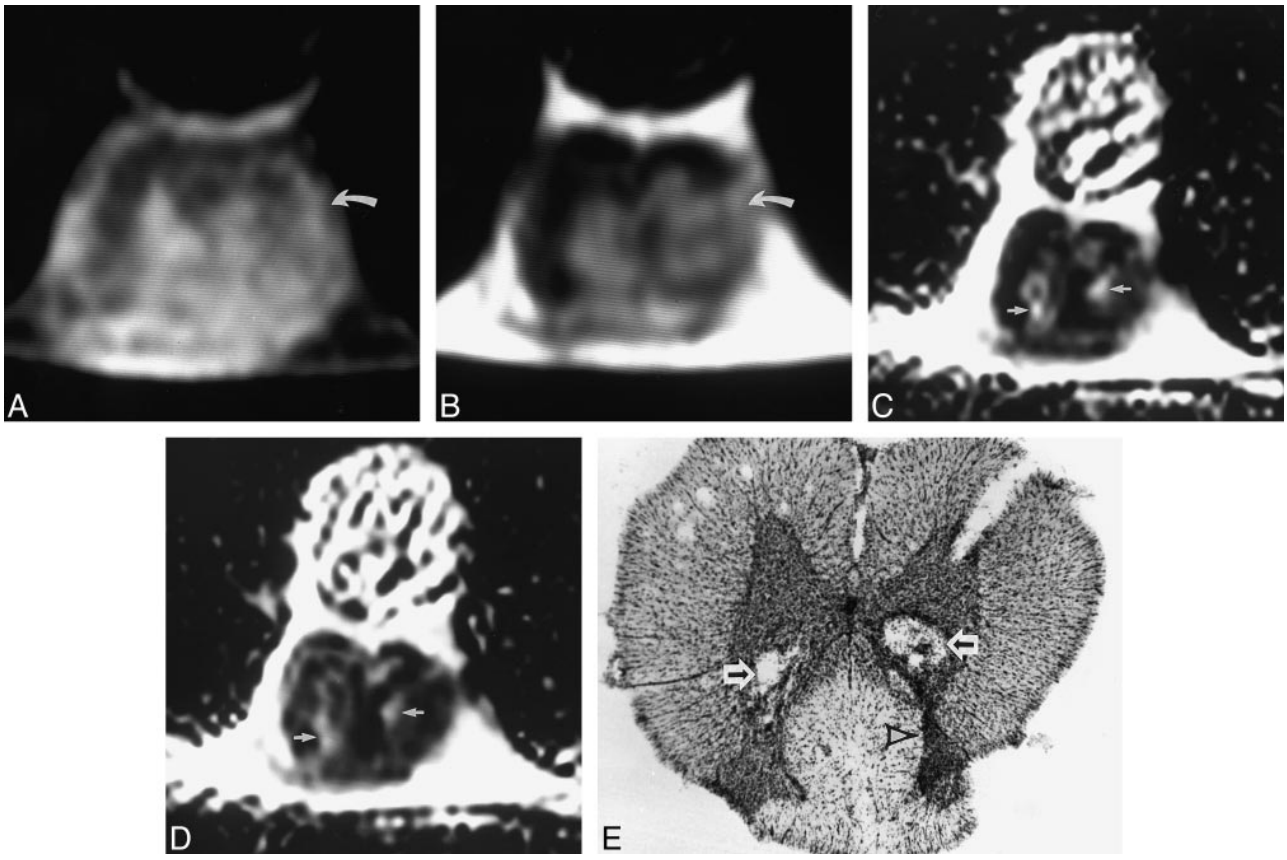

FIG 2. *A–E,* Cross-sectional T1-weighted (800/22/6) (*A*) and T2-weighted (2000/80/4) (*B*) images of rat spinal cord 1 week after injection show abnormal heterogeneous signal in the gray matter, worse on the left, with associated loss of normal gray/white differentiation (*curved arrow*). Corresponding ADC maps in the read (*C*) and slice-select (*D*) axes show two areas of increased signal (*arrows*) in both axes, corresponding to the two cavities partially filled with cellular debris on the histopathologic specimen (*arrows, E*). The increased neuronal damage on the left is seen as a relative decrease in size of the dorsal gray matter on the left side of the spinal cord (*arrowhead*).

was hypointense relative to the gray matter. The signal changes in the white matter were expected, as prior studies have shown that diffusion anisotropy is preserved in fixed specimens (33). The anisotropy corresponded to freer motion of water molecules within axons along the longitudinal axis of the ascending and descending white matter tracts, as compared with the relatively restricted motion of water molecules in the read axis (transverse plane) across axonal walls.

One week after injection, the T1- and T2-weighted images of one of the specimens showed abnormal heterogeneous signal within the gray matter at the level of injection, with loss of gray/white differentiation, worse on the left than the right (Fig 2A and B). No definite cystic lesions were evident; however, the ADC maps in both the slice-select and read axes showed two areas of increased signal intensity (Fig 2C and D), which corresponded to two debris-filled cavities on the histologic specimen (Fig 2E). In addition, there was increased neuronal cell loss on the left as compared with the right, which was seen as decreased size of the ventral horn (Fig 2E); this asymmetric damage was reflected on the conventional MR images (Fig 2A and B). The other specimen imaged 1 week after injection similarly displayed no cystic lesions on conventional MR images, and the ADC maps again showed increased signal intensity corresponding to cavities on the histologic specimen (not shown).

At 4 weeks, T1- and T2-weighted images showed an area of low T1 and high T2 signal in the center of the spinal cord (Fig 3A and B). These signal characteristics were consistent with a spinal cord cyst. This lesion corresponded to an area of increased signal intensity on both ADC maps (Fig 3C and D). In a corresponding histopathologic section, a central cystic lesion was seen with relatively less debris than apparent in the lesions seen at 1 week (Fig 3E). In addition, there was a thicker, more well-defined cellular border to this lesion, suggesting the characteristics of a cyst. Finally, a linear area of low signal intensity was seen in the dorsal gray matter on both the T1- and T2-weighted images (Fig 3A and B), which represented neuronal degeneration, gliosis, and scarring along the injection tract (Fig 3E). Similar findings of a spinal cord cyst depicted with conventional MR imaging and ADC maps were apparent in the specimen imaged 8 weeks after injection (not shown).

The ADC values of the control gray matter were averaged and the ADC values in areas of increased signal intensity within injected gray matter were also averaged; the white matter was not measured.

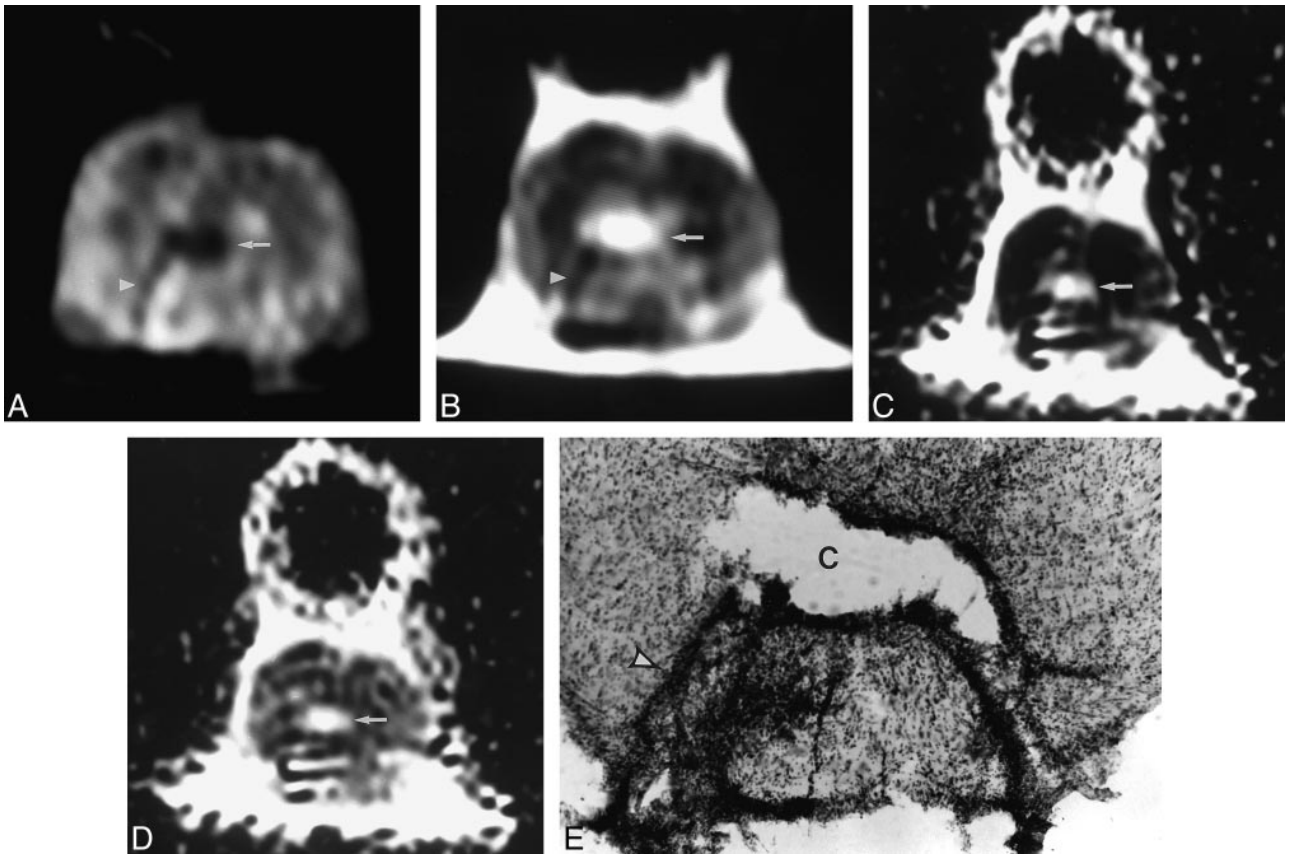

FIG 3. *A–E,* Cross-sectional T1-weighted (800/22/6) (*A*) and T2-weighted (2000/80/4) (*B*) images of rat spinal cord 4 weeks after injection show a cystic lesion within the spinal cord (*arrow*), hypointense on the T1-weighted image and hyperintense on the T2-weighted image. A linear area of low signal intensity on both the T1- and T2-weighted images is seen within the dorsal gray matter (*arrowhead*), representing neuronal degeneration, gliosis, and scarring along the injection tract. Corresponding ADC maps in the read (*C*) and slice-select (*D*) axes show this cystic lesion (*arrow*) to be hyperintense in both axes. The cystic lesion seen on the MR images corresponds to the cyst (C) seen in the histopathologic specimen (*E*), and the glial scarring seen on the conventional MR images is marked with an *arrowhead*; note the decreased amount of debris within the cyst as compared with the cavities seen in Figure 2E.

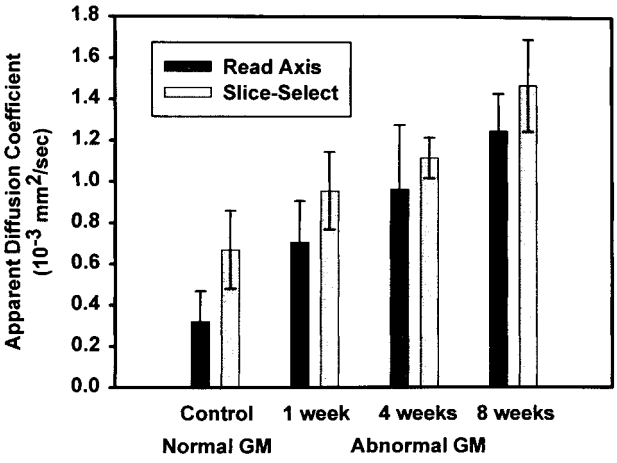

FIG 4. Graph of the ADC values (10^{-3} mm^2/s) in both the read and slice-select axes versus time. There is a progressive increase in ADC values (*y*-axis) of the lesions seen within the affected gray matter as the time (*x*-axis) since injection increased from 1 to 8 weeks.

A graph of the gray matter ADC in both the slice-select and read axes versus time was then plotted (Fig 4). The spinal cord gray matter in the control specimen showed slightly increased values in the slice-select axis as compared with the read axis, which may represent mild diffusion anisotropy along the longitudinal axis. This finding is similar to those obtained in another study using rat spinal cords (30). There was a progressive increase in ADC values of the visualized lesions as the time since injection increased. Statistical analysis with linear regression showed that this progressive increase in ADC values was statistically significant in both the read ($P < .05$) and slice-select ($P < .05$) axes. The gray matter above and below the levels of injury in the injected animals had ADC values similar to that of the control specimen.

Discussion

The indications for treatment of post-traumatic syringomyelia are controversial (1, 9). Some authors advocate neurosurgical treatment when a patient becomes symptomatic, and suggest serial diagnostic studies for asymptomatic patients with

cysts (2, 4, 6, 10). Other authors have argued for prophylactic treatment of spinal cord cysts (34), especially in the cervical spinal cord, where rapid progression of the syrinx may lead to respiratory failure (2). Most authors agree that MR imaging is the best diagnostic radiologic tool, and that early detection of these post-traumatic spinal cord cysts is important to prevent or minimize the effects of syringomyelia (2, 4, 6, 35). In the present study, we evaluated a method of imaging that may provide earlier detection of patients at risk for post-traumatic syringomyelia than available with current clinical MR imaging techniques.

Prior studies of spinal cord injury and cyst formation have used the weight-drop (26–28, 30) or clip-compression methods (29), which have shown abnormal signal intensity within the spinal cord relating to hemorrhage. Subsequent cyst formation may occur after such injuries, although not as consistently as with the animal model of syringomyelia that we used. Our model consistently creates cysts with histologic features that are consistent with post-traumatic spinal cord cysts (21). Although the excitotoxic model of spinal cord injury is a non-traumatic model, it contains many of the pathophysiologic characteristics found after traumatic spinal cord injury, including neuronal loss, gliosis, demyelination, inflammation, breakdown of the spinal blood-brain barrier, and cavitation (21–23, 31). Immunostaining for glial fibrillary acidic factor was positive in border areas of spinal cavities (21), which is consistent with a gliotic border that is expected in post-traumatic syringomyelia (1, 9, 21). For this reason, the excitotoxic model is believed to be relevant to studies related to mechanisms of secondary tissue damage that follow spinal cord injury.

Excitatory amino acids act on multiple receptors in neuronal cell membranes, and with excessive activation can trigger an excitotoxic cascade that ultimately leads to cell death (21). As cells die, there is increased permeability of the blood-brain barrier within the spinal cord, and increased edema. A cavity begins to form as macrophages clear necrotic tissue and reactive astrocytes and fibroblasts wall off the necrotic area within the spinal cord (31). As fluid fills the cavity, perfusion of surrounding tissue may also be affected, and this alteration in spinal cord blood flow may cause ischemia and the increased release of excitatory amino acids, which forms the basis for a destructive cycle of continued tissue damage (16).

In this study, the ADC images at 1 week showed areas of signal intensity that correlated with cavitary changes in pathologic specimens. In addition, the ADC values of these areas were increased. The increase was expected, as cavities and cysts should have freer movement of water molecules. The cavitary changes could not be seen on the conventional T1- and T2-weighted images at this time. At 4 and 8 weeks, conventional MR imaging showed lesions with signal intensities consistent with cyst formation. These lesions corresponded to areas of increased signal intensity on the ADC maps as well as to cystic lesions in the histologic specimens. The increasing ADC values within the areas of increasing signal intensity may represent clearing of necrotic debris and proteinaceous material as cavities become organized into cysts (31). As the injury progresses and debris is removed, there should be increasingly freer movement of water molecules, which is reflected by increasing ADC values in both the slice-select and read axes at 1, 4, and 8 weeks after injury.

There were two limitations associated with our model that need to be mentioned. First, this model does not take into account the effects of arachnoiditis, scarring, and tethering of the spinal cord following injury. The abnormal CSF flow associated with cord tethering may play an important role in cyst progression and may relate to surgical outcome (2, 4, 6–8, 10, 36–41). Cho et al (11) used a rabbit model of syringomyelia that compared the effects of subarachnoid kaolin injection with the weight-drop model. In their study, they showed that subarachnoid kaolin injection alone was not enough to produce definite cysts or cavities, but combining it with the weight-drop model made the animal more prone to develop cysts (55.5%) than with the weight-drop model alone (12.5%). In the rat model we used, cysts developed in 100% of injected animals, and we therefore believe that this rat model of syrinx formation will be useful in the testing of neuroprotective treatment strategies to prevent post-traumatic syringomyelia. Although the excitotoxic model results in the formation of cysts over the 2-month period evaluated in the present study, it remains to be seen whether these cysts will continue to enlarge over more extended periods of time.

The second limitation concerns the need for ex vivo imaging if diffusion-weighted imaging is to be performed. Newer techniques for in vivo MR imaging, such as high-powered gradients and implantable coils (42), may make in vivo diffusion-weighted imaging of the rat spinal cord possible (43–45). These advances will allow the longitudinal study of syrinx formation with diffusion-weighted imaging as well as with conventional imaging (43, 46).

Diffusion-weighted imaging of the in vivo human spinal cord is becoming a reality (47). It should become feasible to create ADC maps in patients with spinal cord injury in order to evaluate early cavity or cyst formation, which may be appreciated with this technique before such lesions are discernible with conventional MR imaging, thus leading to earlier treatment.

Conclusion

Diffusion-weighted imaging with ADC maps may detect early formation of cavitary lesions in the spinal cord before they are visible on conven-

tional T1- and T2-weighted images. This technique may potentially be applied to future animal studies of pathophysiology and to the treatment of posttraumatic syringomyelia. In addition, diffusion-weighted imaging may become a useful clinical tool for the diagnosis and monitoring of secondary pathologic changes, including cavity formation that follows spinal cord injury in humans.

References

1. Green BA, Lee TT, Madsen PW, et al. **Management of posttraumatic cystic myelopathy.** *Top Spinal Cord Inj Rehabil* 1997;2: 36–46
2. Biyani A, Masry WS. **Post-traumatic syringomyelia: a review of the literature.** *Paraplegia* 1994;32:723–731
3. Jinkins JR, Reddy S, Leite CC, et al. **MR of parenchymal spinal cord signal change as a sign of active advancement in clinically progressive posttraumatic syringomyelia.** *AJNR Am J Neuroradiol* 1998;19:177–182
4. Sgouros S, Williams B. **Management and outcome of posttraumatic syringomyelia.** *J Neurosurg* 1996;85:197–205
5. Quencer RM, Sheldon JJ, Post MJ, et al. **MRI of the chronically injured cervical spinal cord.** *AJR Am J Roentgenol* 1986;147: 125–132
6. Schurch B, Wichmann W, Rossier AB. **Post-traumatic syringomyelia (cystic myelopathy): a prospective study of 449 patients with spinal cord injury.** *J Neurol Neurosurg Psychiatry* 1996; 60:61–67
7. Levi ADO, Sonntag VKH. **Management of posttraumatic syringomyelia using an expansile duraplasty.** *Spine* 1998;23:128–132
8. Tanghe HLJ. **Magnetic resonance imaging (MRI) in syringomyelia.** *Acta Neurochir* 1995;134:93–99
9. Madsen PW, Falcone S, Bowen BC, Green BA. **Post-traumatic syringomyelia.** In: Levine A, Eismont F, Garfin S, Zigler J, eds. *Spine Trauma.* Philadelphia: Saunders; 1998;608–629
10. Klekamp J, Batzdorf U, Samii M, et al. **Treatment of syringomyelia associated with arachnoid scaring caused by arachnoiditis or trauma.** *J Neurosurg* 1997;86:233–240
11. Cho KH, Iwasaki Y, Imamura H, et al. **Experimental model of posttraumatic syringomyelia: the role of adhesive arachnoiditis in syrinx formation.** *J Neurosurg* 1994;80:133–139
12. Panter SS, Yam SW, Faden AI. **Alteration in extracellular amino acids after traumatic spinal cord injury.** *Ann Neurol* 1990;27: 96–99
13. Marsala M, Sorkin LS, Yaksh TL. **Transient spinal ischemia in rat: characterization of spinal cord blood flow, extracellular amino acid release and concurrent histopathological damage.** *J Cereb Blood Flow Metab* 1994;14:604–614
14. Liu D, Thangnipon W, McAdoo DJ. **Excitatory amino acids rise to toxic levels upon impact injury to the rat spinal cord.** *Brain Res* 1991: 547;344–348
15. Yezierski RP. **Pain following spinal cord injury: the clinical problem and experimental studies.** *Pain* 1996;68:185–194
16. Madsen PW, Yezierski RP, Holets VR. **Syringomyelia: clinical observations and experimental studies.** *J Neurotrauma* 1994;11: 241–254
17. Faden AI, Simon RP. **A potential role for excitotoxins in the pathophysiology of spinal cord injury.** *Ann Neurol* 1988;23: 623–626
18. Wrathall JR, Choiniere D, Teng YD. **Dose dependent reduction of tissue loss and functional impairment after spinal cord trauma with the AMPA/kainate antagonist NBQX.** *J Neurosci* 1994;14:6598–6607
19. Liu S, Ruenes GL, Yezierski RP. **NMDA and non-NMDA receptor antagonists protect against excitotoxic injury in the rat spinal cord.** *Brain Res* 1997;756:160–167
20. Hao J-X, Xu X-J, Aldskogius H, et al. **The excitatory amino acid receptor antagonist MK-801 prevents the hypersensitivity induced by spinal cord ischemia in the rat.** *Exp Neurol* 1991;113: 182–191
21. Yezierski RP, Santana M, Park S, et al. **Neuronal degeneration and spinal cavitation following intraspinal injections of quisqualic acid in the rat.** *J Neurotrauma* 1993;10:445–456
22. Brewer KL, Bethea JR, Yezierski RP. **Neuroprotective effects of interleukin-10 following excitotoxic spinal cord injury.** *Exp Neurol* (in press)
23. Dancausse HA, Brunschwig JP, Bunge MB, et al. **Morphological characterization of excitotoxic injury in the rat spinal cord.** *Soc Neurosci Abstr* 1995;21:231
24. Bunge RP, Puckett WR, Becerra JL, et al. **Observations on the pathology of human spinal cord injury: a review and classification of 22 new cases with details from a case of chronic cord compression with extensive focal demyelination.** *Adv Neurol* 1993;59:75–89
25. Bunge RP, Puckett WR, Hiester ED. **Observations on the pathology of several types of human spinal cord injury, with emphasis on the astrocyte response to penetrating injuries.** *Adv Neurol* 1997;72:305–315
26. Guizar-Sahagun G, Rivera F, Babinski E, et al. **Magnetic resonance imaging of the normal and chronically injured adult rat spinal cord in vivo.** *Neuroradiology* 1994;36:448–452
27. Falconer JC, Narayana PA, Bhattacharjee MB, et al. **Quantitative MRI of spinal cord injury in a rat model.** *Magn Reson Med* 1994;32:484–491
28. Hackney DB, Ford JC, Markowitz RS, et al. **Experimental spinal cord injury: MR correlation to intensity of injury.** *J Comput Assist Tomogr* 1994;18:357–362
29. Duncan EG, Lemaire C, Armstrong RL, et al. **High-resolution magnetic resonance imaging of experimental spinal cord injury in the rat.** *Neurosurgery* 1992;31:510–519
30. Ford JC, Hackney DB, Alsop DC, et al. **MRI characterization of diffusion coefficients in a rat spinal cord injury model.** *Magn Reson Med* 1994;31:488–494
31. Guizar-Sahagun G, Grijalva I, Madrazo I, et al. **Development of post-traumatic cysts in the spinal cord of rats subjected to severe spinal cord compression.** *Surg Neurol* 1994;41:241–249
32. Carvlin MJ, Asato R, Hackney DB, et al. **High-resolution MR of the spinal cord in humans and rats.** *AJNR Am J Neuroradiol* 1989;10:13–19
33. Pattany PM, Puckett WR, Klose KJ, et al. **High resolution diffusion-weighted MR of fresh and fixed cat spinal cords: evaluation of diffusion coefficients and anisotropy.** *AJNR Am J Neuroradiol* 1997;18:1049–1056
34. Small JA, Sheridan PH. **Research priorities for syringomyelia: a National Institute of Neurological Disorders and Stroke workshop summary.** *Neurology* 1996;46:577–582
35. Quencer RM. **Can MR help predict enlargement of posttraumatic spinal cord cysts?** *AJNR Am J Neuroradiol* 1998;19:192
36. Quencer RM, Bunge RP. **The injured spinal cord: imaging, histopathologic, clinical correlates, and basic science approach to enhancing neural function after spinal cord injury.** *Spine* 1996; 21:2064–2066
37. Asano M, Fujiwara K, Yonenobu K, et al. **Post-traumatic syringomyelia.** *Spine* 1996;21:1446–1453
38. Milhorat TH, Capocelli AL, Anzil AP, et al. **Pathological basis of spinal cord cavitation in syringomyelia: analysis of 105 autopsy cases.** *J Neurosurg* 1995;82:802–812
39. Tobimatsu Y, Nihei R, Kimura T, et al. **A quantitative analysis of cerebrospinal fluid flow in post-traumatic syringomyelia.** *Paraplegia* 1995;33:203–207
40. Quencer RM, Donovan Post MJ, Hinks RS. **Cine MR in the evaluation of normal and abnormal CSF flow: intracranial and intraspinal studies.** *Neuroradiology* 1990;32:371–391
41. Post MJD, Quencer RM, Hinks RS, et al. **Spinal CSF flow dynamics: qualitative and quantitative evaluation by cine MR.** Presented at the annual meeting of the American Society of Neuroradiology, Orlando, March 1989
42. Wirth ED, Mareci TH, Beck BL, et al. **A comparison of an inductively coupled implanted coil with optimized surface coils for in vivo NMR imaging of the spinal cord.** *Magn Reson Med* 1993;30:626–633
43. Ford JC, Hackney DB, Joseph PM, et al. **A method for in vivo high resolution MRI of rat spinal cord injury.** *Magn Reson Med* 1994;31:218–223
44. Nakada T, Matsuzawa H, Kwee IL. **Magnetic resonance axonography of the rat spinal cord.** *Neuroreport* 1994;5:2053–2056
45. Matsuzawa H, Kwee IL, Nakada T. **Magnetic resonance axonography of the rat spinal cord: postmortem effects.** *J Neurosurg* 1995;83:1023–1028
46. Wise Y. **Letter.** *Neurosurgery* 1992;31:517–519
47. Holder CA, Eastwood JD, Muthupillai R, et al. **Diffusion-weighted MR imaging of the normal human spinal cord in vivo.** Presented at the annual meeting of the American Society of Neuroradiology, Philadelphia, May 1998